HHS Public Access

Author manuscript

Nature. Author manuscript; available in PMC 2014 March 13.

Published in final edited form as:

Nature. 2013 September 12; 501(7466): 185–190. doi:10.1038/nature12464.

RNAi screens in mice identify physiological regulators of oncogenic growth

Slobodan Beronja, **Peter Janki**, **Evan Heller**, **Wen-Hui Lien**, **Brice Keyes**, **Naoki Oshimori**, and **Elaine Fuchs**[1]

Howard Hughes Medical Institute, Laboratory of Mammalian Cell Biology & Development, The Rockefeller University, New York, New York 10065, USA

Summary

Tissue growth is the multifaceted outcome of a cell's intrinsic capabilities and its interactions with the surrounding environment. Decoding these complexities is essential for understanding human development and tumorigenesis. Here, we tackle this problem by carrying out the first genome-wide RNAi-mediated screens in mice. Focusing on skin development and oncogenic ($Hras^{G12V}$-induced) hyperplasia, our screens uncover novel as well as anticipated regulators of embryonic epidermal growth. Among top oncogenic screen hits are Mllt6 and the Wnt effector β-catenin; they maintain $Hras^{G12V}$-dependent hyperproliferation. We also expose β-catenin as an unanticipated antagonist of normal epidermal growth, functioning through Wnt-independent intercellular adhesion. Finally, we document physiological relevance to mouse and human cancers, thereby establishing the feasibility of *in vivo* mammalian genome-wide investigations to dissect tissue development and tumorigenesis. By documenting some oncogenic growth regulators, we pave the way for future investigations of other hits and raise promise for unearthing new targets for cancer therapies.

Genome-wide cellular RNAi screening has advanced the identification of genes involved in oncogenic growth control. To date, however, high throughput screens in mammalian cells have been limited to cultures, which even for the best systems, incompletely model physiological environments. We've overcome this impediment by devising methods to efficiently and selectively transduce murine epidermis through *in utero* lentiviral targeting of progenitors in E9.5 embryos[1]. When coupled with shRNA expression, lentiviral

[1]To whom correspondence should be addressed: Elaine Fuchs, Howard Hughes Medical Institute, Laboratory of Mammalian Cell Biology & Development, The Rockefeller University, 1230 York Avenue, Box#300, New York, NY, 10065, USA., Phone: 212-327-7953, Fax: 212-327-7954, fuchs@rockefeller.edu.

Supplementary Information is linked to the online version of the paper at www.nature.com/nature.

Author Contributions S.B., P.J. and E.F. designed the experiments. S.B. and P.J. made shRNA pools and lentivirus, and performed the screens. Illumina sequence analysis was done by E.H. and S.B. RNAseq and IPA analyses were performed by S.B., B.K. and P.J. Imaging was done by S.B. and N.O., and image analysis by S.B. and E.H. CHIP-seq data was generated by W.H.L, and P.J performed luciferase assays. S.B. and E.F. wrote the paper. All authors provided intellectual input, vetted and approved the final manuscript.

Author Information Reprints and permissions information is available at www.nature.com/reprints. Raw RNAseq data can be accessed at Gene Expression Omnibus (GSE#48480).

The authors declare no competing financial interest.

transduction is stably propagated throughout skin epithelium, resulting in RNAi-mediated reductions in target transcript and protein levels. This enables rapid analysis of complex genetic pathways in mammals, something previously only possible in lower eukaryotes[2-4].

The correlation between a tissue's growth and turnover rates and its susceptibility to cancer makes embryonic epidermis an attractive model for exploring how rapidly growing tissues balance proliferation and differentiation, and what prevents them from doing so in tumor progression. Given the efficacy of our system to single gene studies, we've now expanded this scale by >four orders of magnitude to conduct genome-wide RNAi screens. Our objectives were to first, demonstrate the feasibility of such screens in mammals; second, identify epidermal growth regulators in their native, physiological environment; third uncover how epidermal growth control changes when it is propelled by a well-known oncogene; and fourth, demonstrate the implications of our findings for tumor progression in mice and humans.

Epidermal growth is rapid and uniform

Following completion of gastrulation and continuing to birth, mouse surface ectoderm commences rapid growth to match embryo expansion (Fig. 1a). Beginning as a monolayer, E9.5 ectoderm differentiates into a stratified, multi-layered epidermis that by birth constitutes a barrier that retains fluids and excludes microbes. Mature epidermis maintains an inner progenitor layer, which fuels tissue homeostasis and wound repair.

To quantify epidermal growth, we randomly marked single cells at clonal density by infecting E9.5 Rosa26$^{\text{lox-stop-lox-yfp}}$ Cre-reporter embryos (*r26*$^{yfp/+}$)[5] with an LV-Cre lentivirus[1], and then monitored their expansion during development (Fig. 1b). By E18.5, single YFP$^+$ cells at E10.5 had grown to clones constituting ~40 cells (Fig. 1b,c; ~5-6 divisions/cell). Variability in clone size ranged within 1-2 cell divisions, indicating strikingly uniform growth throughout the epidermis.

We next examined how growth is affected by oncogenic *Hras1*, found mutated in many cancers and the primary target in skin carcinogenesis models[6,7]. *K14*-Cre[8] driven, epidermal-specific expression of G12V-Hras from its endogenous locus (Hras$^{\text{Lox-WT-STOP-Lox-G12V}}$)[9] resulted in mice whose skin displayed epidermal overgrowth as well as oncogenic Hras dose-dependency for one (*K14-Cre; Hras*$^{LSL\text{-}G12V/+}$; Hras$^{\text{oncoX1}}$) or two copies (*K14-Cre; Hras*$^{LSL\text{-}G12V/LSL\text{-}G12V}$; Hras$^{\text{oncoX2}}$) (Supplementary Fig. 1). Additional distinctions included expansion of both progenitors (keratin 5+) and differentiating layers (spinous, keratin 10+; granular, filaggrin+) (Supplementary Figs. 1-3).

To quantify the impact of oncogenic Hras on epidermal growth, we used a Cellular Growth Index (CGI) assay[1] (Fig. 1d). Cre-reporter (*r26*$^{yfp/+}$) embryos, transduced with LV-Cre and RFP-expressing lentivirus (LV-RFP) mix showed similar relative numbers of YFP$^+$ to RFP$^+$ keratinocytes across several embryos, indicating that control YFP$^+$ and RFP$^+$ populations grew at comparable rates (Fig. 1e,f). Transduction of the same lentiviral mixture into test animals (where Cre-transduction induces Hras^{G12V}) revealed consistently more YFP$^+$ (Hras^{G12V}) than RFP$^+$ (control) cells (CGIs=1.82, one copy; 3.32, two copies Hras^{G12V};

Figs. 1e,f). These findings demonstrate that $Hras^{G12V}$ confers a dose-dependent growth advantage to skin epidermis and that growth rates can be documented and quantified.

$Hras^{G12V}$ not only conferred a dose-dependent increase in proliferation, but also in suppression of apoptosis (Supplementary Fig. 4). Additionally, consistent with established pro-inflammatory effects of $Hras^{G12V}$, innate and adaptive immune cells infiltrated underlying dermis. Lastly, real-time PCR revealed no evidence for oncogenic induction of cellular senescence-associated CDK inhibitors[10].

Establishing pooled screen parameters

Based upon the principle of our CGI assay, we expected that following epidermal transduction with a pool of shRNA-expressing lentivirus, any shRNA that targets an essential mediator of growth will be reduced or lost during development, while shRNAs targeting negative growth regulators will become overrepresented. By comparing relative shRNA abundance in the initial pool and at E18.5, we expected to identify shRNAs and their targets that confer either growth advantage or disadvantage.

The success of the approach depended upon our ability to: a) modify growth at a low Multiplicity of Infection (MOI ≤ 1), b) measure individual shRNA abundance in the pool, c) transduce embryonic epidermis at an MOI ≤ 1, and d) achieve complete screen coverage, where every shRNA in the pool is tested. We set up a series of controls to ensure that these parameters are met. Underscoring the feasibility of pooled-formats for *in vivo* RNAi screens, we demonstrated that targeting of a) anaphase promoting complex component *Anapc5* during normal growth, and b) *Hras1* during oncogenic hyperplasia, significantly reduced average clone sizes, even with transductions where most cells harbored only a single shRNA (Supplementary Fig. 5).

To quantify individual shRNA representation in a complex pool, we used the Illumina-based count-by-sequencing principle (Supplementary Fig. 6). We designed oligonucleotides to amplify the target sequence of each shRNA, and optimized pre-amplification and clean-up pipelines to yield a product to apply directly to the sequencing cell. We tested our protocol against a defined template generated by combining genomic DNAs from independently transduced cell lines, so that individual genome-integrated shRNAs were present in amounts corresponding from a single cell (6pg) up to 2,048 cells (12.3ng).

We amplified and sequenced this standard set, and showed that reactions were: a) quantitative, with increased sequencing reads corresponding to shRNA abundance in the pool, b) sensitive, detecting all three single-copy shRNAs, and c) highly reproducible (Supplementary Fig. 6). Independent counts of the standard set showed identical sequencing bias for a given shRNA, and thus became neutralized in relative comparisons of absolute counts, especially with ≥32 copies of the shRNA. Indeed, a >30-fold screen coverage proved sufficient to sample all shRNAs in our pool (see below). At this level, growth-neutral shRNAs were >1,000-fold represented in the E18.5 sequencing quantification reaction, since each E9.5 epidermal cell generates ~40 cells by E18.5.

We next determined that at an infection level of 13-27%, most transduced epidermal keratinocytes carried a single lentivirus (MOI≤1) (Supplementary Fig. 7). To ensure that at least 30 individual cells were infected with each shRNA at E9.5, a pool of ~78,000 shRNAs required ~10^6 cells to be targeted. We used high-resolution imaging of TOPRO3-labeled embryos and established that at E9.5, surface ectoderm contained ≥120,000 cells/embryo. Together, this suggested that transducing ≥90 embryos would achieve the requisite coverage (Supplementary Fig. 8).

Screens identify known growth regulators

We pooled the genome-wide collection of murine shRNA lentiviruses in roughly equal concentrations[11], and profiled the starting composition of the pool (t=0), in transduced primary mouse keratinocytes (Fig. 2a). Physiological screens were performed in control and $Hras^{oncoX2}$ embryos transduced at E9.5 *in utero* (Fig. 2b). Epidermal cells were collected after 24hrs (initial pool) and 9d of development, and integrated lentiviral hairpins from genomic DNAs were sequenced and quantified (Fig. 2c).

Our pre-amplification and sequencing reactions did not bias shRNA quantification, and Illumina sequencing reads were of high quality. They mapped to the shRNA library with predictable efficiency and indicated complete coverage of the pool (Supplementary Fig. 9,10). Significantly altered shRNAs were identified and ranked based on two independent methods. To ensure reproducibility, we used DESeq statistical package[12], which accounted for biological variability among our replicates (sets of 30 embryos/condition) and is the best method to identify candidates per se (Fig. 2d-k). However, informative yet variable shRNAs can be excluded by the high stringency of DESeq, which reduces the ability to control for off-target effects by requiring that multiple shRNAs show consistent behavior. We therefore also analyzed pooled data sets (90 embryos/condition; Supplementary Fig. 11) using Fisher's exact test, which reduces variability by averaging individual shRNA abundance. By maximizing screen coverage, this method produces a more inclusive list of significantly altered shRNAs, and hence was preferred for ranking candidates identified by DESeq (Fig. 2f,j,k). Importantly, the overlap between these approaches was extensive (Supplementary Fig. 11), underscoring the robustness of our data.

We identified ~1,800 genes as essential for normal growth (Fig. 2d,e, Supplementary Table 1,2), and were significantly enriched for function in protein synthesis (*P*=3.1E-10) and gene expression (*P*=2.6E-10). Genes encoding 60S and 40S ribosomal proteins were also highly represented and among the top 10% of all hits for normal growth, underscoring our screen's power to identify regulators of normal growth/viability (Fig. 2f, Supplementary Fig. 12). Indeed our top 10 candidates for regulators of normal growth featured six ribosomal genes and two genes essential for mRNA splicing (Fig. 2j).

In our screen for specific regulators of $Hras^{G12V}$-dependent oncogenic growth, ~160 genes surfaced as candidates (Fig. 2g, Supplementary Table 3,4). They diverged in identity and function from those implicated in normal growth regulation, as most housekeeping growth regulators were eliminated by pair-wise comparison of control and $Hras^{oncoX2}$ shRNA abundance (Fig. 2h). The oncogene-specific regulators included Hras1, and downstream Ras

pathway members Raf1, MEKs, and Akts (Fig. 2i). Equally notable was the absence of upstream oncogenic Ras regulators, e.g. guanine nucleotide exchange factors (GEFs) and GTPase-activating proteins (GAPs), which are not expected to arise in a screen for hairpins suppressing $Hras^{G12V}$-induced growth. Our top 10 hits for regulators of oncogenic growth included well-established Ras pathway members *Akt3* and *Raf1*, as well as the Ras-regulated *Pawr*[13] (Fig. 2k). Cyclin C (*Ccnc*), a putative regulator of hematopoietic stem cell quiescence[14] was also on this list, as was *Mllt6*, encoding an MLL translocation partner in acute leukemia and a component of an epigenetic modifier complex[15].

The very top candidate for preferential regulation of oncogenic growth was *Ctnnb1*, encoding the Wnt signaling and intercellular adhesion effector β-catenin. At first glance, β-catenin seemed obvious, as its over-activation has been implicated in a variety of cancers, including those of skin[16-18]. However, β-catenin is also thought to be essential for stem cells[19]. Hence, it was surprising that its hairpins surfaced in a screen for *selective inhibitors* of oncogenic and not normal growth. Even more paradoxical was that in our parallel genome-wide screen, *Ctnnb1* was the top candidate for negative regulation of normal epidermal growth (Supplementary Table 1,2).

Validating oncogene-specific regulators

We chose *Ctnnb1* and *Mllt6* for further study. For both *Ctnnb1* and *Mllt6*, a direct correlation was observed between transcript knockdown *in vitro* and severity of growth defects *in vivo* (Supplementary Fig. 13), strongly arguing against off-target effects. We validated our candidates as oncogenic growth regulators with a modified *in vivo* CGI assay involving two lentiviral vectors (Fig. 3a). In one, Cre-recombinase fused to monomeric RFP (LV-Cre::mRFP) contained a scrambled shRNA control. In the other vector, untagged Cre was used; this vector encoded the test shRNA against the candidate. Transduction of E9.5 control or $Hras^{oncoX2}$ Cre-reporter embryos marked two separate populations: RFP^+YFP^+ cells represented the baseline rate of normal (in control) or oncogenic growth (in $Hras^{oncoX2}$); YFP^+ cells represented the rate of growth that occurs when the target transcript is depleted.

The ratios of YFP^+ cells normalized to YFP^+RFP^+ cells in $Hras^{oncoX2}$ and control animals revealed that two independent *Ctnnb1* shRNAs displayed reductions of ~2-4-fold in oncogenic relative to normal growth. Similar ~two-fold reductions in YFP^+ cells were observed in the $Hras^{oncoX2}$ background when *Mllt6* transcripts were diminished (Fig. 3b). The physiological effects of *Ctnnb1* or *Mllt6* knockdown were profound: the neonatal oncogenic phenotype was significantly ameliorated, and epidermal proliferation in $Hras^{oncoX2}$ embryos was markedly and reproducibly suppressed. By contrast, no significant effects were seen on apoptosis (Fig. 3c, Supplementary Fig. 13).

Equally interesting to the selective effects of *Ctnnb1* knockdown on suppressing $Hras^{G12V}$-dependent oncogenic growth were its positive effects on normal growth. These differences appeared physiologically significant, as they were reflected at the level of EdU-incorporation and thickness of epidermal tissue (Fig. 3c, Supplementary Fig. 14). Although

hitherto overlooked, the proliferative effects of *Ctnnb1* hairpins on normal epidermis are recapitulated upon conditional targeting of β-catenin[20,21].

β-Catenin is both an adherens junction component and a nuclear cofactor for Wnt-regulators LEF/TCF and other DNA binding proteins[22]. However in contrast to its nuclear functions, β-catenin's role in adhesion has been assumed to be redundant with plakoglobin[23]. Given that intercellular defects can promote proliferation, we revisited this issue using a sensitive *in vitro* adhesion assay (Fig. 3d-f, Supplementary Fig. 15)[24]. Despite plakoglobin upregulation, *Ctnnb1*-null keratinocytes inefficiently formed cell-cell adhesions upon calcium induction. Moreover, the Wnt inhibitor XAV939[25] failed to phenocopy these defects. Finally, consistent with the view that loss of β-catenin compromises contact-inhibition and leads to cellular overgrowth, *Ctnnb1*-null cells were hyperproliferative and formed overgrown foci upon reaching confluence.

Oncogenic growth and Wnt signaling

Although intercellular adhesion is often viewed as tumor-suppressive, Wnt signaling is often associated with oncogenic growth. To test whether this might contribute to the negative effects of *Ctnnb1* knockdown on $Hras^{G12V}$ skins, we transduced embryos with both a Wnt-reporter and LV-Cre (Fig. 4a). In E18.5 control animals, reporter expression was predictably restricted to developing hair follicles[26] and largely abolished with concomitant *Ctnnb1* knockdown.

Intriguingly, Wnt-reporter expression was expanded throughout transduced $Hras^{oncoX2}$ interfollicular epidermis. Additionally, $Hras^{G12V}$-expressing epidermis displayed ectopic nuclear β-catenin and >6-fold upregulation of *Axin2* transcripts (Fig. 4a; Supplementary Fig. 16a-c). Conversely, BMP signaling, which is antagonistic to Wnt signaling in skin[27], was downregulated in $Hras^{GV12}$ epidermis, and was not rescued by β-catenin depletion, suggesting its independence of Wnt in this oncogenenic context (Supplementary Fig. 18).

Mllt6 expression paralleled β-catenin and Wnt reporter activity, both in normal hair follicles and in evaginating structures of $Hras^{oncoX2}$ skin (Supplementary Fig. 16b). Chromatin immunoprecipitation followed by next-generation sequencing (ChIP-seq) analysis showed that TCF3 and TCF4 bound to a conserved LEF/TCF motif upstream of *Mllt6* (Fig. 4b). A 299bp segment (green line) encompassing this site drove LEF1/β-catenin-dependent luciferase reporter activity in a manner comparable to the 331bp TCF3/4 binding site of *Axin2*, an established Wnt-target gene (Fig. 4c; Supplementary Fig. 16d). In agreement, depletion or loss of β-catenin in embryonic epidermis *in vivo* reduced *Mllt6* transcript levels (Fig. 4d).

β-catenin and Mllt6 in epidermal tumors

Although our screens were conducted on embryonic mouse skin, our findings showed relevance to cancer. RNA-seq analysis revealed that *Ctnnb1* or *Mllt6* depletion in oncogenic Hras epidermis affected a shared set of transcripts (P=2.48E-40 and P=8.16E-25) that globally suppressed pathways promoting tumorigenesis (e.g. *Myc, E2f1*) and enhanced those restricting growth (e.g. *Trp53, Cdkn2a*; Fig. 4e,f). Moreover in human squamous cell

carcinomas (SCC), β-catenin and Mllt6 were often upregulated and nuclear (notably in the basal layer, where cancer stem cells reside[28]). Our analysis of 75 different human skin SCCs showed that most tumors expressed both proteins, with significant correlation in their expression (Supplementary Fig. 18). It remains to be seen whether their co-expression in tumors and a shared effect on transcriptional profile during oncogenic growth reflects a functional interaction between our candidates, or is a result of their independent effect/importance on the cellular machinery at the heart of oncogenic growth.

We next tested whether β-catenin and Mllt6 are physiologically relevant to $Hras^{G12V}$-dependent tumor initiation and maintenance. While clonal LV-Cre-mediated activation of $Hras^{G12V}$ expression in mice resulted in squamous papilloma formation as early as three weeks of age, concomitant constitutive expression of *Ctnnb1* or *Mllt6* shRNAs delayed tumor initiation (Fig. 5a). Moreover, growth of orthotopically transplanted SCC cells was significantly reduced following candidate depletion (Fig. 5b; Supplementary Fig. 19).

We extended this physiological relevance by performing xenografts of human SCC cells transduced with lentivirus harboring scrambled or shRNAs targeting h*Ctnnb1* or h*Mllt6*. Tumor initiation was significantly delayed, with *Mllt6* showing stronger effect than *Ctnnb1* (Fig. 5c; Supplementary Fig. 19).

Finally, to assess whether *Ctnnb1* and *Mllt6* are required for tumor maintenance, we engineered an LV-Cre vector that allows for doxycycline-regulated shRNA expression, thereby enabling induced depletion of *Mllt6* and *Ctnnb1* following tumor formation in adult animals (Fig. 5d, Supplementary Fig. 20). Both had negative effects on tumor maintenance, with some tumors showing partial regression. Thus, the tumor-suppressive effects of *Ctnnb1* and *Mllt6* shRNAs as first revealed in embryogenesis appeared to be functionally relevant to adult tumorigenesis.

Discussion

The urgent need to understand cancer has fueled human cancer genome sequencing and *in vitro* RNAi-based screening efforts to identify genes that preferentially affect cancer cells but not their normal counterparts. While promising in concept, assay conditions and cell-line histories can profoundly affect genes identified in these screens[29,30]. Although xenogeneic transplantations of transduced human cells offer improvements[31], they often incompletely simulate carcinoma ontogeny, which depends upon complex interactions with local and systemic environments. By targeting cells in their normal physiological context, we correct these deficits and abrogate many caveats, including epigenetic, genetic, and stress-induced alterations in gene expression, all of which introduce heterogeneity and increase coverage requirements when cells are grown on plastic.

Our study accentuates a particular importance of β-catenin in promoting oncogenic effects, since it surfaced at the top of >15,000 genes in our screen. Moreover, elevated Hras-MAPK signaling drove β-catenin's effects from negative to positive, since normal epidermal growth was actually impeded by β-catenin. In this regard, it is interesting that leukemias also seem to be more sensitive to activated β-catenin than their normal counterparts[32]. Our findings

further suggest that β-catenin's ability to balance tissue growth is exerted through its antagonistic functions in intercellular adhesion and transcriptional activation.

A myriad of new candidates from our screen await further investigation. Among them are chromatin modifiers, which have been increasingly implicated in human cancers[33]. In this regard, our validation of Mllt6 is intriguing, since MLL proteins are known to associate with DotL1 H3K79-methyltransferase complexes[34]. Given Mllt6's selective effects on oncogenic growth, it is tempting to speculate that this protein might function by guiding its histone modifier complex to a key cancer target gene(s). While detailed understanding of this and other candidates awaits experimentation, our methodology paves the way for future studies aimed at uncovering mechanisms of SCC progression, with the hope of identifying targets that selectively compromise growth of one of the world's most prevalent and life-threatening cancers.

Methods

Lentivirus production and in vivo and in vitro transductions

Large-scale production and concentration of lentivirus were performed as previously described[1]. Male and female animals was used in equal numbers, and all mice were on the C57BL/6 background, including *Gt(ROSA)26Sor*$^{tm1(EYFP)Cos/+}$ (Jackson Laboratories, donated by A. McMahon), *FR-Hras*^{G12V} (9), and *Tg(K14-Cre)1Efu*[8]. Mice were housed and cared for in an AAALAC-accredited facility, and all animal experiments were conducted in accordance with IACUC-approved protocols. Randomization and blinding were not used in this study. Detailed description of the *in vivo* lentiviral transductions can be found elsewhere[1,35]. For lentiviral infections in culture, cells were plated in 12-well dishes at 70,000 cells/well and incubated with lentivirus in the presence of polybrene (100 mg/ml) overnight. After 2 days, infected cells were sorted based on RFP expression (mouse and human SCC cells) or positively selected with puromycin (1 mg/ml) for 4 days and processed for mRNA analysis.

mRNA quantifications

Total RNAs were isolated from FACS-sorted cells from E18.5 epidermis or from flash-frozen, pulverized kidney, using the Absolutely RNA Microprep kit (Stratagene). cDNAs were generated from 1 μg of total RNA using the SuperScript Vilo cDNA synthesis kit (Life Technologies). Real-Time PCR was performed using the 7900HT Fast Real-Time PCR System (Applied Biosystems) and gene-specific and *Ppib* control primers. Real-time experiments were done on cells isolated from 3 transduced animals, or 3 independently transduced cell culture plates, and all reactions were performed in triplicate and in two separate runs. BRE-Zs-Green activity was measured using Real-Time PCR with *ZsGreen* specific primers on cDNA from transduced epidermal cells as previously described[4].

Immunostaining and histological analyses

The following primary antibodies were used: chicken anti-GFP (1:2,000; Abcam); mouse anti β-catenin (15B8, 1:1,000; Sigma); guinea pig: anti-K5 (1:500; E. Fuchs); rat anti-CD34 (RAM34, 1:100; eBioscience), anti-Ecad (ECCD-1, 1:200; M. Takeichi), and anti-Nidogen

(ELM1, 1:2,000; Santa Cruz); rabbit anti-Caspase 3 (AF835, 1:1,000; R&D), anti-RFP (PM005, 1:2,000; MBL), anti-K10 (PRB-159P, 1:1,000; Covance), anti-Filaggrin (PRB-417P, 1:2,000; Covance), anti-pSmad1/5/8 (AB3848, 1:1,000; Millipore), and anti-Mllt6 (NBP1-89222, 1:100; Novus Biologicals). Secondary antibodies were conjugated to Alexa-488, 546, or 647 (1:1,000, Life Technologies). Detection of pSmad1/5/8 was enhanced using the Tyramide Signal Amplification (Perkin Elmer). Cells and tissues were processed as previously reported[1], and mounted in ProLong Gold with DAPI (Life Technologies). Skin squamous cell cancer tissue array (SK802a) was obtained from US Biomax Inc. Immunohistochemistry preparations were developed using ImmPRESS Universal Antibody Polymer Detection method (Vector Laboratories). Confocal images were captured by a scanning laser confocal microscope (LSM510 and LSM780; Carl Zeiss, Inc.) using Plan-Apochromat 20x/0.8 oil and C-Apochromat 40×/1.2 water lenses. Images were processed using ImageJ and Adobe Photoshop CS3. To quantify the number of ectodermal cells at E9.5, embryos were fixed in 4% paraformaldehyde, permeabilized in PBS + 0.1% Triton (Sigma), and the nuclei were labeled with TO-PRO-3 as recommended (Life Technologies). Tiled Z-stack images of were collected on a Zeiss LSM780 using a Plan-Apochromat 63×/1.4 oil lens. Stacks and metadata were imported into MATLAB (Mathworks Inc.) using the LOCI Bio-Formats Importer[36]. For each stack, the surface was located by finding the first Z position with an average intensity 3-fold above background, and the stack was cropped to 6 μm corresponding to the surface epithelium. The resulting images were segmented in 3D using Imaris (Bitplane AG) to obtain counts of nuclei.

Flow cytometry

Primary epidermal keratinocytes were isolated[37] and then purified by fluorescence activated cell sorting (FACS) using BD FACSAria II (BD Biosciences). Nucleotide analogue EdU (50mg/g body weight) was injected intraperitoneally 2 hrs prior to processing, and EdU (Life Technologies) incorporation and active Caspase-3 (BD Pharmingen) assays were performed as recommended. Immune cell infiltration was analyzed in whole skin dissociated with a sequential incubation in collagenase (Sigma; 0.25% in HBSS for 90 min) and trypsin (Gibco; 0.25% in PBS for 15 min) at 37 °C. The following biotin-conjugated rat antibodies (1:100; Pharmingen) were used: anti-CD11b (M1/70), anti-CD103 (M290), anti-Ly-6G/C (RB6-8C5), anti-CD3e (145-2C11), anti-CD45 (30-F11), and anti-CD45R (RA3-6B2). YFP/RFP quantification was based on detection of the native protein in unfixed cells. Flow cytometric analysis was performed on BD LSR II.

Cell culture assays

Cells were cultured in 0.05 mM Ca^{2+} (E18.5 mouse epidermal keratinocytes and SCC cells) or 1.5 mM Ca^{2+} (human SCC) E-media supplemented with 15% serum. Cell adhesion in primary epidermal keratinocytes seeded at low confluence was assayed by replacing their growth medium with a 1.5 mM Ca^{2+} E-media, and fixing them at different times thereafter. Nucleotide analogue EdU (10 μM) was added to cell culture media 90 min prior to processing, and contact inhibition was analyzed in cells 3 days after reaching confluence. Inhibition of Wnt signalling was achieved by addition of 5 μM Tankyrase inhibitor XAV939 [IC50 values 11 nM (Tnks1) and 4 nM (Tnks2)] to the media 12 hrs before the start of the experiments.

Lentiviral constructs

Sequences of RNAi constructs are listed in Supplementary Table 5. Design of LV-RFP, LV-GFP and LV-Cre has been previously reported[1]. Lentiviral construct for inducible shRNA expression is a modification of tet-pLKO-puro[38] (Addgene plasmid 21915), where the IRES-Puro cassette was replaced between the *XmaI* and *KpnI* sites with the ligation of PCR-amplified *XmaI*/*NheI* flanked *P2A* fragment and *NheI*/*KpnI* flanked *nlsCre* cDNA. The lentiviral Wnt reporter was fashioned after the lentiviral Beta-catenin Activated Reporter[39]. It includes 12 *Tcf/Lef* binding sites followed by a minimal TK promoter and an *mRFP1* transgene that were subcloned into a pLKO.1 backbone between *KpnI* and *NheI* sites. Lentiviral BMP-reporter that contains a pair of BMP response elements is a derivative of BRE-ZsGreen[4], where the *reporter* cassette between *XhoI* and *NheI* sites has been placed between SalI and NheI sites of the pLKO-nlsCre-MCS vector.

Tumor free survival

Control and $Hras^{oncoX2}$ animals were transduced at E9.5 with low-titre LV-Cre containing constitutively expressing or inducible shRNA against Scrambled control or test *Ctnnb1* and *Mllt6* shRNAs. Transductions were confirmed by real-time PCR of P7 (newborn) littermates, and the remaining animals were monitored for an additional 12 weeks. Animals were assessed every 2-3 days, and scored positive when tumors were larger than 2 mm in diameter. Animals transduced with an LV-Cre containing inducible shRNAs were allowed to form tumors for 60 days, at which point individual tumors were measured along their short and long axis using a digital caliper (t=0). Next, tumor-bearing animals were treated by a single IP injection of Doxycycline (100 μl of 50 mg/ml) and maintained on Doxycycline containing chow for 8 weeks, and tumor size was assayed every 7 days. Because the tumor volumes at t=0 showed a range between 4-20 mm^3, the assayed tumor size was normalized to the initial tumor volume, and expressed as fold-change over time. Transplantation of SCC cells transduced with control shRNA, or shRNAs targeting mouse and human Ctnnb1 and Mllt6, into immuno-compromised Nude recipients were performed as previously described[28], and animals were monitored every 3 days for a month. Tumor size was measured using a digital caliper, and tumor volume was calculated using the formula $[(\text{length} \times \text{width})^2 \times \pi]/6$.

TCF3/4 CHIP seq and luciferase assay

Details of the TCF3/4 CHIP seq will be reported elsewhere. For luciferase assays, passage 9-14 293FT cells were seeded in 96-well culture plates and transfected at 60-70% confluence using standard calcium phosphate procedures. Cells were co-transfected with control Renilla pRL-TK, and combinations of 50 ng pGL3-Mllt6, $Mllt6^{mutant}$, Axin2, or $Axin2^{mutant}$ and 200 ng of K14-expression vectors encoding Lef1, ΔNβcat, or control (empty vector). After 44 hours, cells were harvested and luciferase activity was measured using the TD-20/20 luminometer (Turner Biosystems) and the Dual-Glo Luciferase Assay System (Promega). Each transfection was performed in duplicate and repeated 7 times.

Sample preparation and pre-amplification

Epidermal cells were isolated from E18.5 mouse skin using previously established procedures[37]. Cells from individual embryos were used for genomic DNA isolation with the DNeasy Blood & Tissue Kit (Qiagen), and each sample was analyzed for target transduction using real-time PCR. gDNAs from 30 transduced embryos were pooled, and 200 μg of the total were used as template in a 10 ml pre-amplification reaction with 21 cycles and Phusion High-Fidelity DNA Polymerase (NEB). PCR products were run on a 2% agarose gel, and a clean ~200 bp band was isolated using QIAquick Gel Extraction Kit as recommended by the manufacturer (Qiagen). Final samples were then sent for Illumina HiSeq 2000 sequencing.

Sequence processing and relative shRNA quantification

For each genotype, DNA from 30 embryos was pooled and independently sequenced using custom forward (5′-aatgatacggcgaccaccgagatctacactctttccctacacgacgctcttccgatctatatcttgtggaaaggacgaaacacc-3′) and reverse (5′-caagcagaagacggcatacgagctcttccgatctaattgtggatgaatactgccatttgtc-3′) oligos. Illumina reads were trimmed to the 21 nt hairpin sequence using the FASTX-Toolkit and aligned to the TRC 2.x library with BWA (v 0.6.2)[40] using a maximum edit distance of 3. Putative growth regulators were identified by combining two methodologies. First, Illumina reads from 3 sets of 30 embryos were treated as independent biological replicates in the DESeq R package[12]. Dispersions (variability) for each hairpin were estimated using a local fit to the data for each genotype, and hairpins with a p-value < 0.05 by the negative binomial test were considered for downstream analysis. Second, an analysis was carried out on a pooled data set in which the reads from 3 sets of embryos were combined to maximize screen coverage and average biological variability. Although this precludes estimation of within-group variability, it has the effect of reducing noise for poorly counted hairpins when operating close to the minimum required screen coverage. Fisher's exact test was applied on a per-hairpin basis using combined reads by assembling a 2×2 contingency table[41]. The columns of the table are the treatment conditions (e.g. control and $Hras^{oncoX2}$), and the rows correspond to the sequencing counts for a given hairpin in the first, and the counts for all other hairpins in the pool in the second. The test thus calculates the probability of observing a difference in hairpin representation relative to the expected representation in the pool. We further adjust the p-value for multiple testing using the Benjamini-Hochberg correction. Hairpins with a p-value < 0.05 were considered for further analysis. A gene was considered significantly enriched or depleted if at least 2 hairpins exhibited a 2-fold or greater change in normalized reads with a significant p-value, and no hairpins in the set exhibited a change of equal magnitude in the opposite direction. Hits common to both analyses were ranked by number of significant hairpins and the magnitude of their effect. All analyses were carried out in the R statistical enviroment[42], with some plots produced using the ggplot2 package[43]. Gene lists were imported into the Ingenuity Pathway Analysis software (Ingenuity Systems), and analyses and graphic outputs of relative enrichment in functional gene categories were performed as recommended.

Choice of statistical analysis of relative shRNA abundance

The strength of the Fisher's exact test is that it can calculate a probability of observing a difference in shRNA representation in a comparison of pooled data sets. When operating close to the minimum required screen coverage or when it is not feasible to perform many independent replicates, this strategy can be advantageous to increase coverage and reduce noise if combined with additional stringent criteria (i.e. requiring a gene to be targeted by multiple hairpins) and validation.

Because this methodology does not explicitly account for sample-to-sample variability (instead maximizing coverage and averaging out variability), we independently analyzed our data using two additional statistical methodologies that directly address variability within biological replicates. Importantly, both of these methods employed the same stringent set of thresholds (2-fold change in hairpin count, and a requirement for least 2 hairpins to show a significant effect in same direction, and none in the opposite). First, we utilized DESeq[12], an R package designed for the analysis of Illumina sequencing-based assays, which estimates and accounts for biological variability in a statistical test based on the negative binomial distribution. Second, we treated independently sequenced sets of 30 embryos as biological replicates, and generated replicate-specific lists of candidate genes. Comparison of hits shared between these replicates to the hits identified in our analysis of pooled samples yielded a highly conserved set of candidate genes consistent with strong reproducibility of our data. Both analyses identify a list of candidates that substantially overlaps with those identified by our pooling and ranking scheme, with nearly all of our top hits identified regardless of the methodology.

When conducting shRNA drop-out screens, perhaps the most important criteria in identifying potential candidates is that a gene be targeted by multiple, independent hairpins to avoid off-target effects. We thus felt our data would be best-served by combining an analysis of pooled data, which tends to be more inclusive at the level of hairpins and enables ranking by number of independent hairpins, and the results of DESeq, which ensures reproducibility of hits.

RNAseq and IPA network analyses

Epidermal progenitors were FACS sorted into TrizolLS (Invitrogen) and RNA was purified using Direct-zol RNA MiniPrep kit (Zymo Research) per manufacturer's instructions. Quality of the RNA was determined using Agilent 2100 Bioanalyzer, with all samples passing the quality threshold of RNA integrity numbers (RIN)>8. Library preparation using Illumina TrueSeq mRNA sample preparation kit was performed at the Weill Cornell Medical College Genomic Core facility, and cDNA was sequenced on Illumina HiSeq 2000. Reads were mapped to mm9 build of the mouse genome using TopHat, and transcript assembly and differential expression were determined using Cufflinks[44]. Differentially regulated transcripts were analyzed in IPA (Ingenuity Systems), and the upstream transcriptional regulators were predicted using the Upstream Regulator Analysis package, with a significant overlap between the dataset genes and transcription factor targets set at $p<0.01$, and the regulation direction (activated or inhibited) at z-score=2.

Statistics

All quantitative data were collected from experiments performed in at least triplicate, and expressed as mean ± standard deviation (s.d.) or standard error of the mean (s.e.m.). The fits of cellular and tumor growth were compared using the extra sum-of-squares F-test, and expression of Ctnnb1 and Mllt6 in human SCC tissue was analyzed using a non-parametric (Spearman) correlation. Differences between groups were assayed using two-tailed student t-test using Prism 5 (GraphPad Software). Significant differences were considered when $P<0.05$.

Supplementary Material

Refer to Web version on PubMed Central for supplementary material.

Acknowledgements

We thank J. Fagin for inducible oncogenic Hras mice; S. Williams, M. Schober, A. Rodriguez Folgueras, S. Dewell, and D. Schramek for intellectual input; D. Oristian and N. Stokes as mouse specialists; Comparative Bioscience Center (AAALAC accredited) for care of mice in accordance with National Institutes of Health (NIH) guidelines; Genomics Resource Center (C. Zhao, director) for sequencing; Bioimaging Center (A. North, director) for advice; Flow Cytometry facility (S. Mazel, director) for FACS sorting. E.F. is an Investigator of the Howard Hughes Medical Institute. This research was supported by grants from the NIH (R37-AR27883, E.F., K99-AR061469, S.B.), Emerald Foundation (E.F) and Human Frontiers Science Program Postdoctoral Fellowship (S.B.).

References

1. Beronja S, Livshits G, Williams S, Fuchs E. Rapid functional dissection of genetic networks via tissue-specific transduction and RNAi in mouse embryos. Nat Med. 2010; 16:821–827. [PubMed: 20526348]
2. Williams SE, Beronja S, Pasolli HA, Fuchs E. Asymmetric cell divisions promote Notch-dependent epidermal differentiation. Nature. 2011; 470:353–358. [PubMed: 21331036]
3. Ezratty EJ, et al. A role for the primary cilium in Notch signaling and epidermal differentiation during skin development. Cell. 2011; 145:1129–1141. [PubMed: 21703454]
4. Oshimori N, Fuchs E. Paracrine TGF-beta signaling counterbalances BMP-mediated repression in hair follicle stem cell activation. Cell Stem Cell. 2012; 10:63–75. [PubMed: 22226356]
5. Srinivas S, et al. Cre reporter strains produced by targeted insertion of EYFP and ECFP into the ROSA26 locus. BMC Dev Biol. 2001; 1:4. [PubMed: 11299042]
6. Karnoub AE, Weinberg RA. Ras oncogenes: split personalities. Nat Rev Mol Cell Biol. 2008; 9:517–531. [PubMed: 18568040]
7. Balmain A, Pragnell IB. Mouse skin carcinomas induced in vivo by chemical carcinogens have a transforming Harvey-ras oncogene. Nature. 1983; 303:72–74. [PubMed: 6843661]
8. Vasioukhin V, Degenstein L, Wise B, Fuchs E. The magical touch: genome targeting in epidermal stem cells induced by tamoxifen application to mouse skin. Proc Natl Acad Sci U S A. 1999; 96:8551–8556. [PubMed: 10411913]
9. Chen X, et al. Endogenous expression of Hras(G12V) induces developmental defects and neoplasms with copy number imbalances of the oncogene. Proc Natl Acad Sci U S A. 2009; 106:7979–7984. [PubMed: 19416908]
10. Serrano M, Lin AW, McCurrach ME, Beach D, Lowe SW. Oncogenic ras provokes premature cell senescence associated with accumulation of p53 and p16INK4a. Cell. 1997; 88:593–602. [PubMed: 9054499]
11. Moffat J, et al. A lentiviral RNAi library for human and mouse genes applied to an arrayed viral high-content screen. Cell. 2006; 124:1283–1298. [PubMed: 16564017]

12. Anders S, Huber W. Differential expression analysis for sequence count data. Genome Biology. 2010; 11:R106. [PubMed: 20979621]
13. Donninger H, et al. The Ras effector RASSF2 controls the PAR-4 tumor suppressor. Mol Cell Biol. 2010; 30:2608–2620. [PubMed: 20368356]
14. Miyata Y, et al. Cyclin C regulates human hematopoietic stem/progenitor cell quiescence. Stem Cells. 2010; 28:308–317. [PubMed: 19967789]
15. Prasad R, et al. Leucine-zipper dimerization motif encoded by the AF17 gene fused to ALL-1 (MLL) in acute leukemia. Proc Natl Acad Sci U S A. 1994; 91:8107–8111. [PubMed: 8058765]
16. Gat U, DasGupta R, Degenstein L, Fuchs E. De Novo hair follicle morphogenesis and hair tumors in mice expressing a truncated beta-catenin in skin. Cell. 1998; 95:605–614. [PubMed: 9845363]
17. Chan EF, Gat U, McNiff JM, Fuchs E. A common human skin tumour is caused by activating mutations in beta-catenin. Nat Genet. 1999; 21:410–413. [PubMed: 10192393]
18. Malanchi I, et al. Cutaneous cancer stem cell maintenance is dependent on beta-catenin signalling. Nature. 2008; 452:650–653. [PubMed: 18385740]
19. Nusse R. Wnt signaling and stem cell control. Cell Res. 2008; 18:523–527. [PubMed: 18392048]
20. Huelsken J, Vogel R, Erdmann B, Cotsarelis G, Birchmeier W. beta-Catenin controls hair follicle morphogenesis and stem cell differentiation in the skin. Cell. 2001; 105:533–545. [PubMed: 11371349]
21. Nguyen H, et al. Tcf3 and Tcf4 are essential for long-term homeostasis of skin epithelia. Nat Genet. 2009; 41:1068–1075. [PubMed: 19718027]
22. Clevers H, Nusse R. Wnt/beta-catenin signaling and disease. Cell. 2012; 149:1192–1205. [PubMed: 22682243]
23. Posthaus H, et al. beta-Catenin is not required for proliferation and differentiation of epidermal mouse keratinocytes. J Cell Sci. 2002; 115:4587–4595. [PubMed: 12415003]
24. Vasioukhin V, Bauer C, Yin M, Fuchs E. Direct actin polymerization is the driving force for epithelial cell-cell adhesion. Cell. 2000; 100:209–219. [PubMed: 10660044]
25. Huang SM, et al. Tankyrase inhibition stabilizes axin and antagonizes Wnt signaling. Nature. 2009; 461:614–620. [PubMed: 19759537]
26. DasGupta R, Fuchs E. Multiple roles for activated LEF/TCF transcription complexes during hair follicle development and differentiation. Development. 1999; 126:4557–4568. [PubMed: 10498690]
27. Kandyba E, et al. Competitive balance of intrabulge BMP/Wnt signaling reveals a robust gene network ruling stem cell homeostasis and cyclic activation. Proc Natl Acad Sci U S A. 2013; 110:1351–1356. [PubMed: 23292934]
28. Schober M, Fuchs E. Tumor-initiating stem cells of squamous cell carcinomas and their control by TGF-beta and integrin/focal adhesion kinase (FAK) signaling. Proc Natl Acad Sci U S A. 2011; 108:10544–10549. [PubMed: 21670270]
29. Scholl C, et al. Synthetic lethal interaction between oncogenic KRAS dependency and STK33 suppression in human cancer cells. Cell. 2009; 137:821–834. [PubMed: 19490892]
30. Babij C, et al. STK33 kinase activity is nonessential in KRAS-dependent cancer cells. Cancer Res. 2011; 71:5818–5826. [PubMed: 21742770]
31. Zuber J, et al. RNAi screen identifies Brd4 as a therapeutic target in acute myeloid leukaemia. Nature. 2011; 478:524–528. [PubMed: 21814200]
32. Wang Y, et al. The Wnt/beta-catenin pathway is required for the development of leukemia stem cells in AML. Science. 2010; 327:1650–1653. [PubMed: 20339075]
33. Suva ML, Riggi N, Bernstein BE. Epigenetic reprograming in cancer. Science. 2013; 339:1567–1570. [PubMed: 23539597]
34. Bernt KM, et al. MLL-rearranged leukemia is dependent on aberrant H3K79 methylation by DOT1L. Cancer Cell. 2011; 20:66–78. [PubMed: 21741597]
35. Beronja S, Fuchs E. RNAi-mediated gene function analysis in skin. Methods Mol Biol. 2013; 961
36. Linkert M, et al. Metadata matters: access to image data in the real world. J Cell Biol. 2010; 189:777–782. [PubMed: 20513764]

37. Nowak JA, Fuchs E. Isolation and culture of epithelial stem cells. Methods Mol Biol. 2009; 482:215–232. [PubMed: 19089359]

38. Wiederschain D, et al. Single-vector inducible lentiviral RNAi system for oncology target validation. Cell Cycle. 2009; 8:498–504. [PubMed: 19177017]

39. Davidson KC, et al. Wnt/beta-catenin signaling promotes differentiation, not self-renewal, of human embryonic stem cells and is repressed by Oct4. PNAS. 2012; 109:4485–4490. [PubMed: 22392999]

40. Li H, Durbin R. Fast and accurate short read alignment with Burrows-Wheeler transform. Bioinformatics. 2009; 25:1754–1760. [PubMed: 19451168]

41. Auer PL, Doerge RW. Statistical design and analysis of RNA sequencing data. Genetics. 2010; 185:405–16. [PubMed: 20439781]

42. R Research Development Team. R Foundation for Statistical Computing. Vienna, Austria: 2012. R: A language and environment for statistical computing. *URL*http://www.R-project.org

43. Wickham, H. ggplot2: Elegant Graphics for Data Analysis. Springer; New York: 2009.

44. Trapnell C, et al. Transcript assembly and quantification by RNA-Seq reveals unannotated transcripts and isoform switching during cell differentiation. Nat Biotech. 2010; 28:511–515.

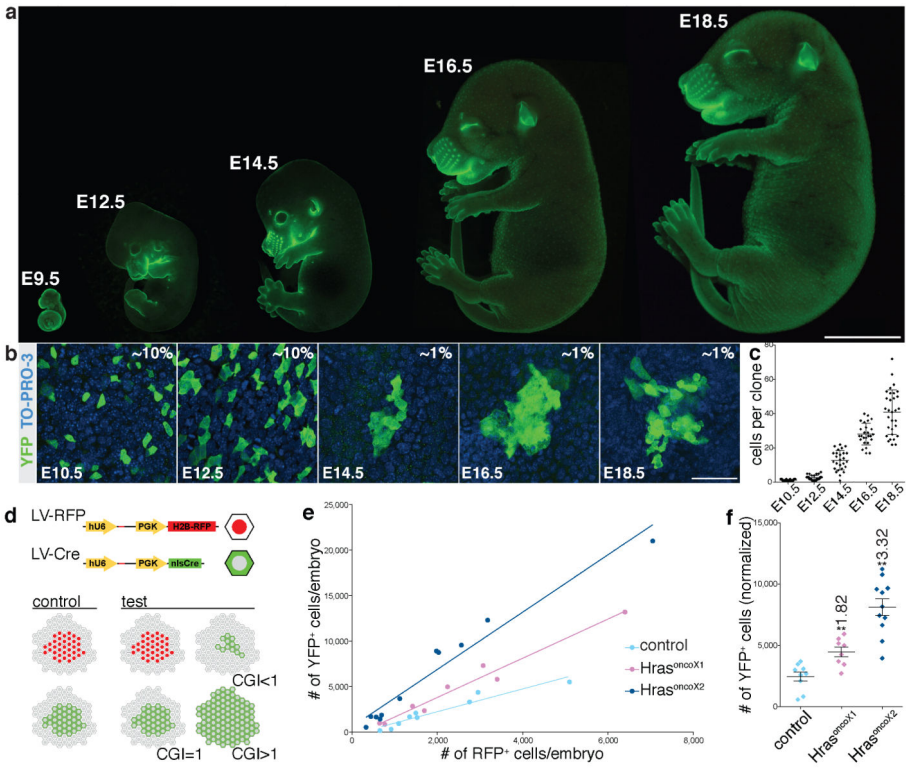

Figure 1. Embryonic epidermal tissue growth is rapid and responsive to oncogenic-Hras

a, Mouse embryogenesis, highlighted by Propidium Iodide (E9.5) or K14-actin::GFP (E12.5-18.5). **b**, *r26*$^{yfp/+}$ Cre-reporter embryos infected at E9.5 with LV-Cre and analyzed at days shown. Transduced cells are YFP^{+}. Transduction levels (% YFP^{+} cells) depend upon viral titre. **c**, Cell numbers in transduced YFP^{+} clones at ages shown. **d**, Schematic of CGI assay. E9.5 *r26*$^{yfp/+}$ Cre-reporter (control) or *gene*$^{lox/lox}$ *r26*$^{yfp/+}$ (test) embryos are infected with LV-Cre and LV-RFP mix. At E18.5, numbers of RFP^{+}:YFP^{+} cells in control and test animals are compared, and phenotypes scored as neutral (CGI=1), growth advantaged (CGI>1) or disadvantaged (CGI<1). **e**, Numbers of RFP^{+} and YFP^{+} cells at E18.5 in control, Hras^{oncoX1}, and Hras^{oncoX2} embryos. Upper shift is consistent with growth advantage. **f**, RFP^{+} cell numbers normalized to YFP^{+} cells in control, Hras^{oncoX1}, and Hras^{oncoX2} animals. CGI assay suggests a 1.8-fold overgrowth (P=0.002) in Hras^{oncoX1}, and 3.3-fold overgrowth (P<0.0001) in Hras^{oncoX2} epidermis. Error bars indicate s.d (**c**) and s.e.m (**f**). For CGI assay (**e,f**), data points are individual embryos: control (n=9), Hras^{oncoX1} (n=8), Hras^{oncoX2} and (n=11). **f**, ** (P≤0.01) indicates statistical significance of comparison to control. Scale bars, (**a**) 5 mm, (**b**) 50 μm.

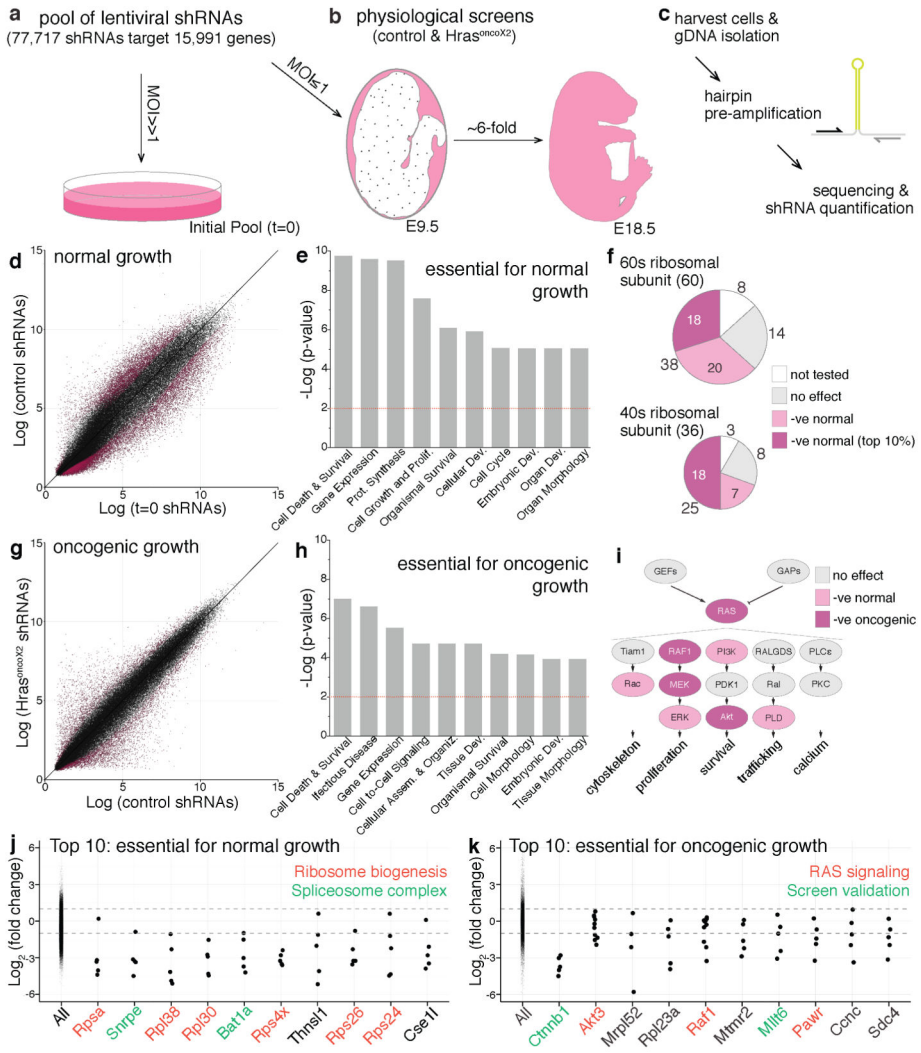

Figure 2. Genome-wide RNAi screens for physiological regulators of normal and oncogenic growth identify expected and surprising regulators

a-c, Schematic of the RNAi screens based on relative enrichment/depletion of individual shRNAs over time. **a**, shRNAs against 15,991 mouse genes are combined into a lentiviral pool whose composition is determined from the "Initial Pool" (t=0) experiment, where transduced cells are analyzed 24 hours after infection. **b**, Genes that regulate normal and oncogenic growth are identified in two screens, in which E9.5 control or K14-Cre^{+}; Hras^{oncoX2} embryos are infected *in utero*, allowed to develop 9d, and processed. **c**, After epidermal tissues are harvested and used in gDNA isolation, individual shRNAs are pre-amplified and quantified by sequencing unique hairpin regions. **d-k**, Significantly enriched/depleted shRNAs identified using DESeq analysis. **d**, Dot plot of relative abundance of 77,717 shRNAs at t=0 and in E18.5 epidermis. **e**, Putative normal growth regulators are significantly enriched (P≥0.01) for gene function categories promoting cell viability and development. **f**, Normal growth regulators encode for ribosomal 60S and 40S subunit components (P=1.12E-09 and P=3.26E-07), with many in the top 10% of all hits (maroon). **g**, Relative shRNA abundance in control and Hras^{G12V} animals reveal oncogenic growth

altering shRNAs. **h**, Putative oncogenic growth regulators are enriched ($P \geq 0.01$) in gene categories that support cell growth. **i**, Downstream effectors of Ras signaling score as essential for growth (pink), with many exhibiting an oncogene-specific requirement (maroon). **j**,**k**, shRNAs for the top ten essential regulators of normal (**d**) and oncogenic (**g**) growth are markedly depleted relative to the genome-wide pool (All).

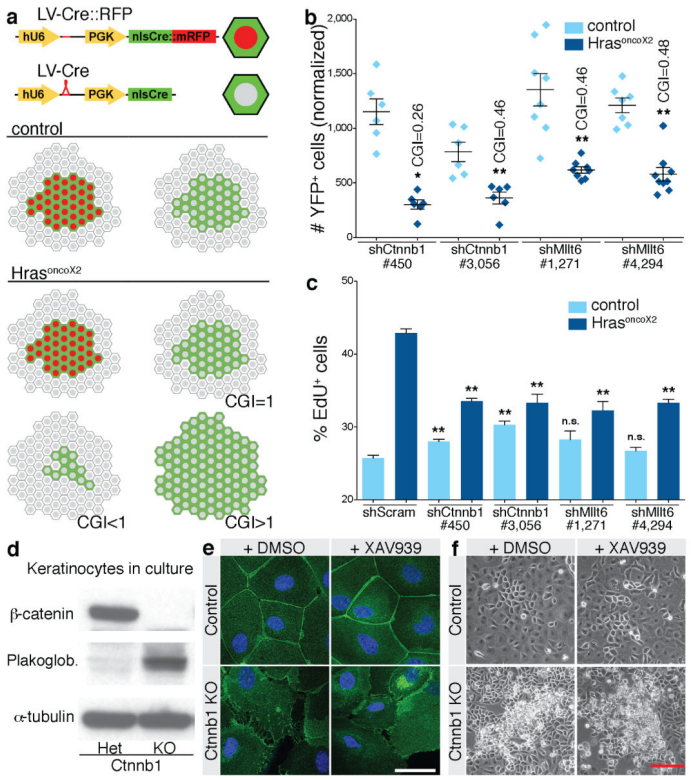

Figure 3. Suppressing β-Catenin and Mllt6 selectively affects Hras^{G12V}-dependent epidermal hyperplasia

a, Modified CGI assay measures effect of shRNA-mediated gene knockdown in animals with Cre-activated transgene expression. Transduction with LV-Cre::RFP co-expressing Scrambled shRNA, and LV-Cre co-expressing candidate-targeting shRNA, leads to generation of YFP^{+}RFP^{+} Scrambled and YFP^{+} knockdown clones in control or Hras^{G12V} animals. Numbers of YFP^{+} cells (normalized to YFP^{+}RFP^{+}) in control and Hras^{oncoX2} animals reflect lentiviral mix composition after normal and oncogenic growth, respectively. **b**, Fewer YFP^{+} cells are found in oncogenic animals upon knockdown of *Ctnnb1* and *Mllt6* with independent shRNAs. **c**, Reduced EdU incorporation following *Ctnnb1* knockdown in Hras^{G12V} animals contrasts with increased proliferation in control epidermis. *Mllt6* depletion also reduces EdU labeling in oncogenic growth. **d**, Immunoblot of control (*Ctnnb1* Het) and *Ctnnb1* KO keratinocyte lysates shows upregulation of Plakoglobin. **e**, Establishment of cell adhesion 48 hrs following Ca^{2+} shift is unaffected in keratinocytes treated with a Wnt-signaling inhibitor (XAV939) but impaired in *Ctnnb1* knockout cells. E-cadherin (green) marks adherens junctions and Dapi (blue) labels the nuclei. **f**, Unlike control cells or cells treated with a Wnt-inhibitor, *Ctnnb1* KO keratinocytes form overgrown foci upon reaching confluence. Error bars (**b**,**c**) indicate s.e.m. Data points (**b**,**c**) represent individual embryos with *n*=6 (shCtnnb1 and shScram in control), *n*=7 (shMllt6#4,294 in control), *n*=8 (shMllt6#1.271), *n*=9 (shMllt6#4,294 in Hras^{G12V}), or *n*=10 (shScram in Hras^{G12V}), each scored through immunofluorescence analysis of ten 425.1 μm^2 images. **b**,**c**, n.s. (not significant, P>0.05), * (P≤0.05), and ** (P≤0.01) indicate statistical significance. Scale bars, (**e**) 50 μm, (**f**) 10 μm.

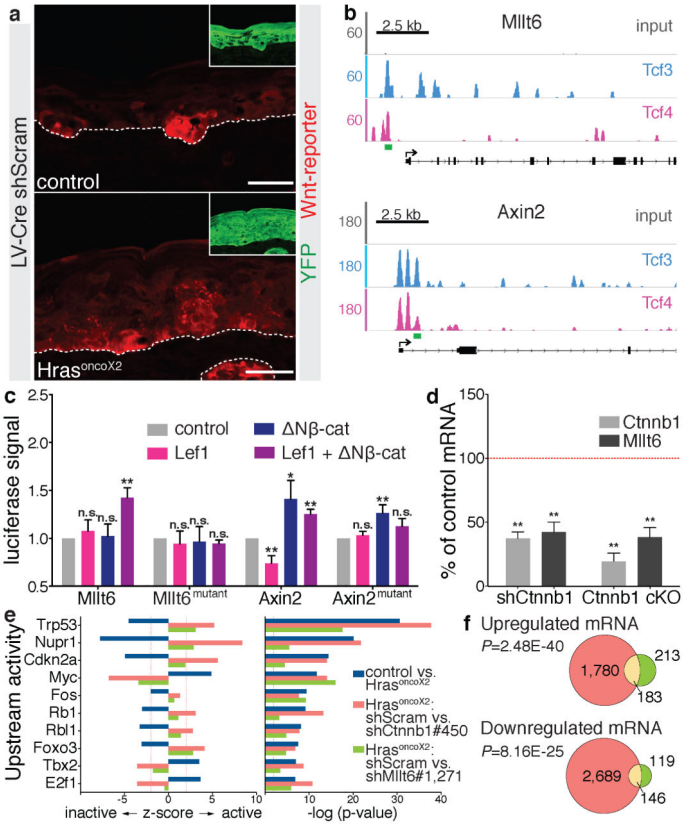

Figure 4. Hras^{G12V}-induced epidermal growth impacts other signaling pathways

a, Wnt-reporter activity is restricted to hair placodes in control skin (top) but extends to interfollicular epidermis in Hras^{oncoX2} animals (bottom). YFP (inset) marks LV-Cre-transduced epidermis. White dotted line demarcates dermal-epidermal boundary. Dapi labels nuclei. **b**, CHIP-seq peaks on chromosome 11 reveal TCF3 (blue) and TCF4 (pink) binding sites in *Mllt6* and *Axin2* promoter regions. Negative control (gray) is total genome DNA. Green bars represent the ~300bp fragment used to validate TCF3/4 binding. **c**, hLEF1 (TCF3/4 family member) and stabilized β-catenin (ΔNβ-cat) together promote luciferase activity when putative TCF3/4 binding sites of *Mllt6* and *Axin2* are used as drivers. These effects are not observed when the TCF3/4 binding motifs are mutated. **d**, *Mllt6* and *Ctnnb1* mRNA epidermal levels are reduced by *Ctnnb1* knockdown (*shCtnnb1#450*) or knockout (cKO). **e**, Transcriptional profile of Hras^{G12V} epidermal progenitors reveals repression of tumor suppressors (eg. TRP53, CDKN2A, RB1) and activation of oncogenic signaling (eg. MYC, E2F1). shRNA-mediated depletion of *Ctnnb1* or *Mllt6* in Hras^{G12V} epidermis significantly counter these transcriptional changes. Red vertical lines represent significant activation z-score (two-fold) and p-value of a correct prediction (p=0.01). **f**, Significant overlap in differentially regulated transcripts is observed following depletion of β-catenin and Mllt6 in Hras^{G12V} epidermal progenitors. Error bars indicate (**c**) s.e.m. and (**d**) s.d. In real-time PCR experiment (**d**), data are shown for three embryos assayed in two independent reactions (n=6). **c**,**d**, n.s. (not significant, P>0.05), * (P≤0.05), and ** (P≤0.01) indicate statistical significance. Scale bar, 50 μm.

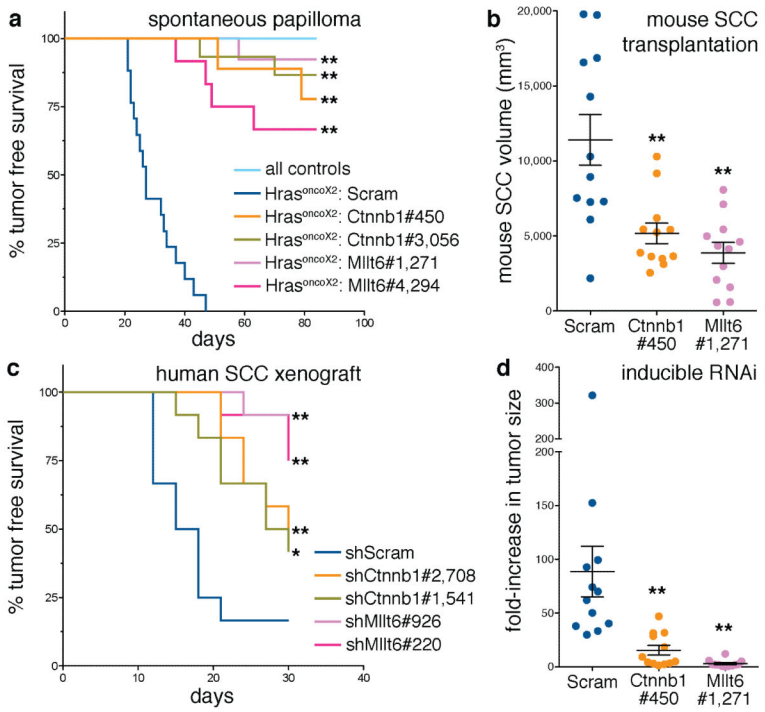

Figure 5. β-catenin and Mllt6 depletion impair Hras^{G12V}-dependent tumorigenesis

a, shRNA-mediated depletion of *Ctnnb1* or *Mllt6* delays spontaneous tumor initiation in Hras^{oncoX2} mice (*n*=9 in all conditions except LV-Scram transduced Hras^{oncoX2} *n*=18). Control lines correspond to animals transduced with shRNAs with no impact on tumorigenesis. **b**, Tumor volume of *Ctnnb1*- and *Mllt6*-depleted mouse SCCs transplants are significantly reduced after 30 days of growth. **c**, Tumor initiation following xenotransplantation of shRNA-transduced human SCC cells is significantly delayed following knockdown of human *Ctnnb1* or *Mllt6*. **d**, Induction of *Ctnnb1* or *Mllt6* knockdown in preexisting spontaneous mouse papillomas results in impaired growth and sometimes regression. **a**-**d**, Transduction of Scrambled shRNA (Scram) served as control. Error bars (**b**,**d**) indicate s.e.m. **b**-**d**, n=12 transplants (**b**,**c**) or tumors (**d**). * (P≤0.05), and ** (P≤0.01) indicates statistical significance of the observed differences.